Feasibility study of measuring the ^{229}Th nuclear isomer transition with ^{233}U-doped crystals

Simon Stellmer, Matthias Schreitl, Georgy A. Kazakov, Johannes H. Sterba, and Thorsten Schumm
Vienna Center for Quantum Science and Technology (VCQ) and Atominstitut, TU Wien, 1020 Vienna, Austria
(Received 23 November 2015; revised manuscript received 13 April 2016; published 5 July 2016)

We propose a simple approach to measure the energy of the few-eV isomeric state in ^{229}Th. To this end, ^{233}U nuclei are doped into VUV-transparent crystals, where they undergo α decay into ^{229}Th, and, with a probability of 2%, populate the isomeric state. These ^{229m}Th nuclei may decay into the nuclear ground state under emission of the sought-after VUV γ ray, whose wavelength can be determined with a spectrometer. Based on measurements of the optical transmission of ^{238}U:CaF_2 crystals in the VUV range, we expect a signal at least two orders of magnitude larger compared to current schemes using surface implantation of recoil nuclei. The signal background is dominated by Cherenkov radiation induced by β decays of the thorium decay chain. We estimate that, even if the isomer undergoes radiative de-excitation with a probability of only 0.1%, the VUV γ ray can be detected within a reasonable measurement time.

DOI: 10.1103/PhysRevC.94.014302

I. INTRODUCTION

The nucleus of ^{229}Th is believed to possess an extremely low-lying excited nuclear state with an energy of only a few eV [1–6]. The notion of applying well-established techniques of optical laser spectroscopy to this nuclear system has encouraged a great number of proposals for possible applications [7–13], among them the development of a nuclear optical clock [8,12,14].

Beginning in the 1970s, a series of γ spectroscopy measurements with ever increasing performance used a differencing scheme to determine the energy of the $J^P[Nn_z\Lambda] = 3/2^+[631]$ isomeric state in an indirect way. The latest measurement places the energy at 7.8(5) eV above the $5/2^+[633]$ ground state [5,15], corresponding to a transition wavelength of 160(10) nm. Predictions of the lifetime of the unperturbed isomeric state range between a few minutes and a few hours [4,16–20], where a value of around 1000 s for a bare nucleus is the most commonly used estimate.

A logical next step in refining the transition wavelength, as well as demonstrating the optical addressibility of this nuclear two-level system, would be optical spectroscopy employing synchrotron radiation on ^{229}Th nuclei doped into, or adsorbed onto [21,22], vacuum ultraviolet (VUV)-transparent crystals. Such crystals allow one to place 10^{16} nuclei into the excitation beam, compared to 10^6 particles in an ion trap [23,24].

The approach of direct optical excitation faces a number of severe challenges: (1) The quantity of ^{229}Th (half life $t_{1/2} = 7932(55)a$ [25]) available for research is very limited, and growing crystals with high Th doping concentrations is a challenge [21]. (2) Both the lifetime and the energy of the isomeric state are known only with large uncertainties [5,21,26], requiring an extensive two-dimensional search. (3) The choice of sufficiently tunable light sources in the VUV range is essentially limited to synchrotrons, where beam time is precious, yet the spectral power is some 11 orders of magnitude smaller compared to diode lasers in the visible range. (4) Photoluminescence in response to the excitation light can persist for long times, potentially masking the nuclear signal [27]. (5) De-excitation of the isomeric state may proceed on parasitic pathways such as internal conversion (IC) and coupling to electronic states and phonons of the crystal, potentially suppressing the optical de-excitation altogether [21,22,28–30]. If de-excitation proceeds via electronic states of the thorium atom, photons at multiple redshifted wavelengths may be observed [29].

The first four of these five challenges can be circumvented by an alternative approach to populate the isomeric state, namely through α decay $^{233}\mathrm{U} \rightarrow {}^{229m}\mathrm{Th}$. Following a cascade of γ transitions, about 2% of the ^{229}Th nuclei end up in the isomeric state [31]. In the absence of competing decay channels, these nuclei will eventually de-excite into the nuclear ground state under emission of the sought-after VUV γ ray. The wavelength of this γ ray can be measured with a spectrometer. Such a spectroscopy experiment could reduce the present uncertainty in the transition wavelength to a degree that would allow one to commence laser spectroscopy.

A number of experiments using ^{233}U recoils have already been performed [32–38], at least two are currently ongoing [6,18,19,39,40]. These experiments are designed such that the detection is well separated in both space and time from the population of the isomer, as the latter process is accompanied by radioactivity and the associated radioluminescence. Commonly, a thin sample of ^{233}U is brought into the vicinity of a UV-transparent crystal (e.g., MgF_2 or CaF_2), such that ^{229}Th recoil nuclei may leave the surface of the ^{233}U source plate and deposit onto, or penetrate slightly into, the absorber plate. The highly energetic momentum recoil of the α decay leaves the ^{229m}Th atom in an uncontrollable electronic state at an unknown position in the crystal lattice. Consequently, the rate of nonradiative de-excitation might be substantially larger compared to a setting of Th ions implanted into a well-defined lattice site using standard crystal growing techniques.

In this article, we investigate an alternative approach, briefly mentioned already in Ref. [41]: ^{233}U-doped crystals as a source of nuclear VUV γ ray emission. The γ ray flux of such crystals may be many hundred times larger compared to surface-implanted ^{229}Th recoils, but the radioactive decay $^{233}\mathrm{U} \rightarrow {}^{229m}\mathrm{Th}$ and the isomer γ ray emission $^{229m}\mathrm{Th} \rightarrow {}^{229g}\mathrm{Th}$ are separated in neither space nor time. This strategy

seems futile at first sight, as an enormous radioluminescence background is introduced into the detection volume. We will show, however, that radioluminescence caused by ^{233}U α decay does not overlap with the anticipated wavelength range around 160 nm. Working towards the interpretation of optical spectra, we find that contaminations of the crystal can generate spectrally narrow features in the UV range, easily misinterpreted as the nuclear isomer signal.

II. PROPOSING A BRIGHT SOURCE OF ISOMER γ ray EMISSION

A number of current experiments use thin foils of ^{233}U, often in the form of UO_2, as a source of ^{229}Th nuclei. An energy of $Q_\alpha = 4.91$ MeV is released upon the α decay of ^{233}U [42], where the ^{229}Th nucleus obtains a recoil energy of up to 84 keV. A Th ion of this kinetic energy has a penetration depth of about 15 nm in UO_2, so if the event occurs close to the surface, and the direction of propagation leads towards the surface, then the Th ion might leave the substrate. The Th ion is caught on a large-band-gap absorber plate. After a certain time of accumulation, the absorber crystal is moved into a detector. This approach thus allows us to separate the ^{233}U α decay and the detection of the VUV γ ray in both space and time.

This method, however, has two severe limitations: At first, the flux of ^{229}Th nuclei that can be implanted into the absorber plate is intrinsically limited by the small range of ^{229}Th recoils in the UO_2 material, and the comparatively long half life of the ^{233}U isotope. The maximum flux of isomeric ^{229m}Th recoil nuclei per unit surface is

$$\Phi = C\,\ell \times \frac{\rho_{UO_2}}{M_{UO_2}} \times N_A \times \frac{\ln(2)}{t_{1/2}} \times R \times B, \qquad (1)$$

where ρ_{UO_2} is the density of the UO_2 and M_{UO_2} its molar mass, $t_{1/2} = 159\,200a$ is the half life of ^{233}U, $\ell \approx 15$ nm is the range of 84-keV recoil ions, and N_A is Avogadro's constant. The geometrical factor $C = 1/4$ accounts for the fraction of nuclei up to a depth of ℓ that reach the absorber plate, and R is the probability of radiative de-excitation. For $R = 1$ and a branching ratio of $B = 2\,\%$, the maximum γ ray emission rate is $\Phi_\gamma \approx 26/(\mathrm{s} \times \mathrm{cm}^2)$.

The second experimental limitation stems from the fact that the penetration of the ^{229}Th ions into the absorber plate is also only a few tens of nanometers. Depending on the surface roughness and cleanliness, the recoil ions might be stopped before reaching the true crystal bulk structure. The band gap of the surface region of the crystal might be smaller than the energy of the isomeric state, allowing it to de-excite via electronic states [28,29].

To overcome these two limitations, we follow a different approach: Doping the ^{233}U directly into a suitable crystal will allow an increase of the production rate of Th recoil ions, and the Th ions will be born directly into the bulk of the lattice. The flux of isomer γ rays that can be extracted from the crystal is intrinsically limited by the optical absorption of uranium defect centers in the crystal. As we will show later, the optical absorption length is equal to $\xi_U(\lambda)/n_U$, where n_U is the uranium doping concentration (in terms of uranium nuclei per crystal unit cell) and $\xi_U(\lambda)$ is a wavelength-dependent material constant. The isomer γ ray flux reads

$$\Phi_\gamma = \xi_U(\lambda) \times \frac{\rho_{crystal}}{M_{crystal}} \times N_A \times \frac{\ln(2)}{t_{1/2}} \times R \times B, \qquad (2)$$

where $M_{crystal}$ denotes the molar mass of a crystal unit cell. Assuming $R = 1$ and the crystal thickness d to exceed the absorption length, $d \gg \xi_U(\lambda)/n_U$, we obtain $\Phi_\gamma \approx 4200/(\mathrm{s} \times \mathrm{cm}^2)$ for ^{233}U:CaF_2. Note that this approach allows for continuous signal integration and does not require knowledge of the isomer lifetime.

III. STUDIES OF FEASIBILITY

To validate our approach, we will now quantify the optical transmission and measure the radioluminescence spectrum of CaF_2 and MgF_2.

A. Crystal transparency

Although U:CaF_2 is widely used as a laser material, transmission curves in the UV spectral range have not been available so far [43,44]. We use an in-house furnace to produce a set of U:CaF_2 crystals with doping concentrations between $n_U = 4.9 \times 10^{-5}$ and 2.0×10^{-3}, corresponding to uranium densities of 1.2×10^{18} cm^{-3} to 4.9×10^{19} cm^{-3}, where we assume a crystal unit cell to be formed by one Ca and two F ions. Due to the radioactivity of ^{233}U and its limited availability, we use depleted ^{238}U as a chemically identical proxy of ^{233}U for the studies presented here. The crystals have a ruby red color, indicating that the uranium atoms are in the trivalent state [44]. The crystals were cut and polished into discs of a few mm thickness and 17 mm diameter.

Transmission measurements were performed with a VUV spectrometer held at a pressure of 2×10^{-6} mbar, where a deuterium lamp is used for calibration and to generate the probe light. Figure 1 shows the transmission curve of a crystal with thickness $d = 4.1$ mm and doping concentration $n_U = 5 \times 10^{-5}$.

We model the transmission as

$$I(\lambda) = I_0\,(1-a)\,e^{-d[1/\xi_{crystal}(\lambda) + n_U/\xi_U(\lambda)]}, \qquad (3)$$

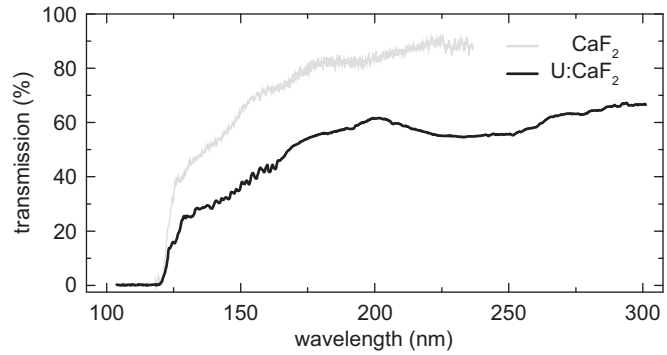

FIG. 1. Transmission of ^{238}U:CaF_2. The black curve was taken with a crystal of $d = 4.1$ mm and $n_U = 5 \times 10^{-5}$, the grey curve shows the transmission of an undoped specimen.

where a describes losses at the crystal surfaces, $\xi_{\text{crystal}}(\lambda)$ accounts for the absorption of an undoped crystal, and $\xi_{\text{U}}(\lambda)$ describes the additional absorption due to the uranium doping. We find that the wavelength-dependent absorption coefficient $\xi_{\text{U}}(\lambda)$ is independent of the doping concentration for values of $5 \times 10^{-5} < n_{\text{U}} < 2 \times 10^{-3}$: the absorption length scales inversely proportional with n_{U}. For a wavelength of 160 nm, we measure $\xi_{\text{U}}(160\ \text{nm}) = 6.3(8) \times 10^{-5}$ cm. It is encouraging to find that this value is 40 times larger than its equivalent quantity ℓ in the approach of recoil implantation.

B. Crystal radioluminescence: CaF_2

A ^{238}U:CaF_2 crystal with an α activity of 1.9 Bq is placed in front of a Cs-Te PMT (sensitivity range 115–320 nm). We record the emission of characteristic bursts of photons, where the rate of the bursts corresponds to the α activity of the ^{238}U. Each burst lasts for a few µs and contains some 10^5 photons [27]. We use a bin width of 10 ms and plot the number of counts per bin in a histogram, shown in Fig. 2. A prominent feature around 120 counts is observed; this feature is associated with the α decay of ^{238}U into ^{234}Th. This isotope quickly decays into ^{234}U (half life 245 000 yr) via two β decays; these β decays are reflected in the hump at about ten counts.

The radioluminescence emission is temperature dependent [45]. We measure a near-linear dependence $\Phi_{\text{RL}}(T) = [1 - c\,(T - T_0)] \times \Phi_{\text{RL}}(T_0)$ between 10 and 80 °C, and obtain a slope of $c = 0.0107(5)\ \text{K}^{-1}$ for $T_0 = 10$ °C. Mild heating from room temperature to 80 °C thus reduces the radioluminescence already by a factor of almost 4. From this characteristic temperature dependence [45], as well as the signature histograms discussed above, we conclude that the radioluminescence properties of U:CaF_2 are governed entirely by the general properties of CaF_2 and are not determined by the uranium doping.

The half life of ^{238}U is too long, and the light throughput of optical spectrometers is too small, to obtain a radioluminescence spectrum from ^{238}U:CaF_2 crystals. As ^{233}U:CaF_2 crystals are not yet available, we simulate such a crystal by bringing a thin layer of ^{233}U [age 45(5) yr, ^{232}U contamination 12(1) ppm] in physical contact with a commercial CaF_2 sample (diameter 25 mm, thickness 5 mm). The ^{233}U had been deposited onto a steel backing using electrodeposition [46], the layer has a diameter of 22 mm, a thickness of about 15 µm, and an activity of 7.5 MBq (1500 times larger compared to the ^{229}Th:CaF_2 crystals used in a related study [27]). Note that only the top 15 nm of the uranium layer give a flux of Th recoil ions into the CaF_2 sample, but the entire thickness contributes α particles and γ rays.

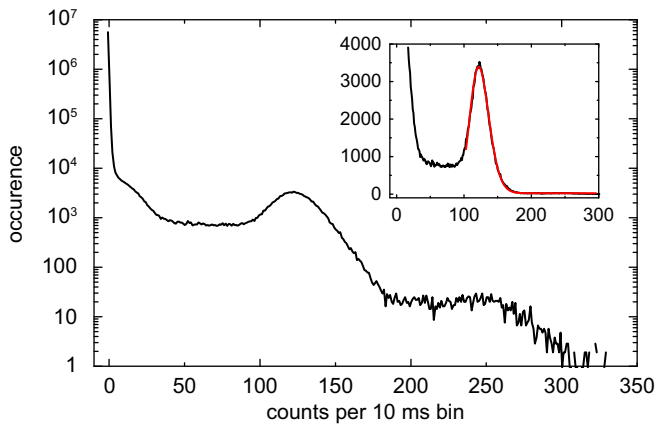

FIG. 2. Histogram of radioluminescence emission from a ^{238}U-doped crystal. The main feature around 120 counts corresponds to a flash of UV photons following α decay, shown also in the inset with a Gaussian fit to the data (red line).

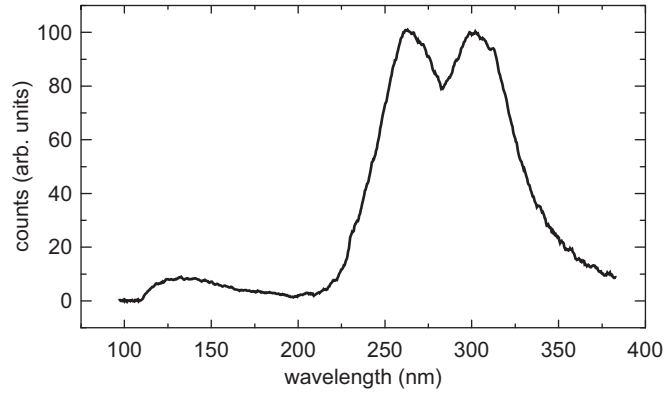

FIG. 3. Radioluminescence of CaF_2 in contact with ^{233}U, showing scintillation between 220 and 400 nm caused predominantly by α decay. The Cherenkov radiation, caused predominantly by β decay of thorium daughters, extends down to the transmission edge of the crystal around 125 nm. The spectrum is not corrected for the wavelength-dependent detection efficiency.

This stack is placed into the spectrometer. The luminescence spectrum, obtained after an integration time of 50 h, is shown in Fig. 3. The spectrum can be decomposed into two parts: the scintillation of CaF_2 around 280 nm [27], and Cherenkov radiation below 200 nm. The spectral shape and amplitude of the scintillation feature depend on the specific type of crystal, as will be discussed in Sec. VI. In CaF_2, it extends down to 220 nm. This finding is very promising, as the scintillation is spectrally far away from the expected isomer wavelength at 160 nm. The scintillation is caused primarily by α particles penetrating the crystal up to a depth of about 15 µm.

The broad spectral component between 120 and 200 nm is attributed to Cherenkov light, caused by β decay of ^{228}Th and ^{229}Th daughters. The cutoff at low wavelengths coincides with the lower transmission edge of the CaF_2 crystal. The Cherenkov light is intrinsically broad and will constitute a locally flat background in the search for the spectrally very narrow isomer signal. Chemical purification of the ^{233}U material prior to crystal fabrication can reduce the Cherenkov light substantially. Note that the amplitude of Cherenkov radiation is proportional to the ingrowth of ^{228}Th and ^{229}Th; this dependence is exactly the same for doped and surface-implanted ions. The signal-to-background ratio of these two approaches is thus identical and depends only on the degree of ^{232}U contamination and on the time elapsed since the last chemical removal of thorium ingrowth from the ^{233}U source material.

An exact calculation of the amount of Cherenkov emission, together with an estimation of experimental parameters, will be given in Secs. IV and V, but we will state the results here. For a time of 100 days since chemical purification, and a ^{232}U contamination of 10 ppm, we calculate an emission of 1.9×10^{-3} Cherenkov photons within a 1.0-nm wavelength window around 160 nm for every ^{233}U decay. Cherenkov emission constitutes a spectrally homogeneous background with Poissonian noise. It is the noise of this background to which the VUV γ ray emission signal needs to be compared to. As a means to quantify the characteristic measurement time, we calculate the integration time needed for the signal to exceed the noise of the Cherenkov background. Assuming $R = 1\%$, $B = 2\%$, $\Phi_\gamma = 4200/(\mathrm{s} \times \mathrm{cm}^2)$, and a standard VUV spectrometer with an overall detection efficiency of 7×10^{-5}, a measurement time T of 1.5 days is required. Note that the time T scales as $(R \times B)^{-2}$.

C. Crystal radioluminescence: MgF_2

Continuing the radioluminescence measurement described above, we now substitute the CaF_2 crystal by MgF_2. The Cherenkov spectrum is smaller in amplitude, as expected from the smaller index of refraction which at 160 nm is 1.55 for CaF_2 and 1.47 for MgF_2. The part of the radioluminescence spectrum that is caused by the impact of massive particles is strikingly different in MgF_2 compared to CaF_2: it consists of only a single broad peak, located at 410 nm, with an amplitude of only 3% compared to the amplitude of the 280-nm peak in CaF_2. This drastic reduction in luminescence, appearing only at higher wavelengths, might be tempting for experiments with insufficient spectral resolution, e.g., using photomultiplier tubes (PMTs).

Crystals made up of light atoms (e.g., LiF, MgF_2) are the preferred choice when x rays are involved, as the x-ray absorption increases drastically with mass number. As an example, the mass attenuation coefficient of MgF_2 is 3.6 times smaller compared to CaF_2 for x rays of 29 keV energy [47].

While uranium doping of LiF has been reported [48], we are not aware of any attempts to grow U:MgF_2 crystals. Measuring the doping efficiency of uranium into MgF_2 is the next step in the assessment of such crystals.

D. Spectrally narrow features

While Cherenkov radiation is intrinsically free of narrow features, crystal contaminations could potentially cause spectrally narrow luminescence. To probe for such disturbing signals, we subject various CaF_2 samples to intense γ radiation inside a shut-down nuclear reactor for 16 h, and measure their luminescence spectra afterwards.

The emission of one specific commercial CaF_2 specimen is shown in Fig. 4(a). On top of a spectrally broad background, we observe two narrow features, the dominant one being located at 312 nm. We monitor the amplitude of this narrow feature over time, and find an exponential decay with a time constant of $\tau = 3.1(1)$ h [right inset of Fig. 4(a)]. The decay of the 275-nm feature and of the background proceeds on the same time scale. The spectral width of this feature is measured to

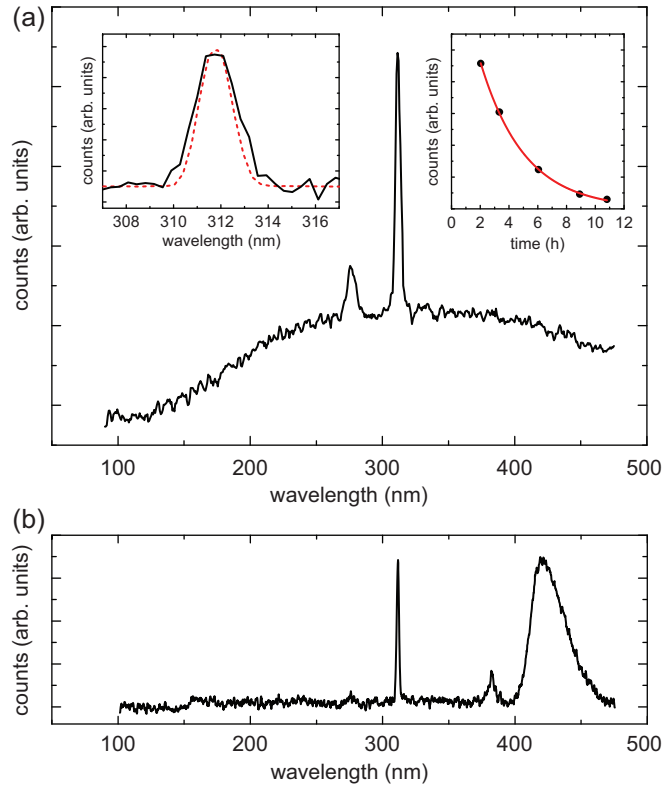

FIG. 4. Long-lived and narrow-bandwidth scintillation of CaF_2 caused by contaminations. (a) Luminescence spectrum of CaF_2 upon irradiation with γ radiation. The narrow feature around 312 nm has a linewidth of less than 1.2 nm and a lifetime of 3.1(1) h; see the text for details. (b) The same narrow feature can be induced by irradiation with VUV light; the feature at 420 nm is caused by F centers.

be 2.05 nm (left inset), largely limited by the instrumental resolution (red dashed line). Subtracting the signal width and the experimental resolution in quadratures, we obtain a natural linewidth of below 1.2 nm. This narrow feature was found in only one batch of crystals from one specific commercial supplier.

The appearance of narrow and long-lived features in the luminescence spectrum of crystals is striking, as typical crystal defects show broad features of typically 10 nm width, and a much faster, nonexponential decay. We attribute the observed features to crystal contamination with Gd^{3+} ions, which show narrow emission at wavelength of 275 and 312 nm [49]. We speculate that crystal defects induced by the γ radiation slowly transfer their energy onto Gd^{3+} ions, which radiate on narrow transitions. These narrow features can also be provoked by illumination with a deuterium lamp; see Fig. 4(b).

Many current experiments search for a spectrally narrow feature with a lifetime on the order of an hour, and use both the linewidth and lifetime to discriminate the isomer signal from the crystal luminescence background. As shown above, contaminations of the crystal can easily be mistaken for the sought-after signal. This pitfall can be circumvented by performing the experiment with different types of crystals. Experiments building on the $^{233}\mathrm{U} \rightarrow {}^{229\mathrm{m}}\mathrm{Th}$ approach could perform reference measurements with ^{234}U, which is very

similar to ^{233}U in terms of half life (245 000 yr vs 160 000 yr), Q_α (4.86 MeV vs 4.91 MeV), and half life of the first daughter nuclei (75 000 yr vs 7932 yr).

IV. CHERENKOV RADIATION

A. Overview

The isomer transition is expected at a wavelength of 160(10) nm, where our approach of ^{233}U-doped crystals is sensitive to the wavelength region between the UV transparency cutoff (125 nm for CaF_2) and the onset of the dominant scintillation features (220 nm in CaF_2, 380 nm in MgF_2). This spectral region is covered by Cherenkov radiation; see Fig. 3. The spectral shape of Cherenkov emission is essentially a convolution of the crystal's transmission, given by $\xi(\lambda)$, and its refractive index $n(\lambda)$, both of which change very smoothly with wavelength. Its amplitude is independent of the specific details of the crystal structure. Cherenkov radiation thus poses a locally homogeneous background rather than a sharp peak that could interfere with the sought-after isomeric signal.

Cherenkov radiation is caused by charged particles (in our case, electrons) traveling through the crystal at velocities v larger than the speed of light in the medium, $v > c/n(\lambda)$, where $n(\lambda)$ is the wavelength-dependent index of refraction. In CaF_2, we find $n(160\ \text{nm}) = 1.55$. The minimum threshold energy required for electrons to emit Cherenkov radiation is

$$E_{e,\min} = m_e c^2(\gamma - 1) \tag{4}$$

with the electron rest mass m_e and the relativistic parameter $\gamma = 1/\sqrt{1-\beta^2}$. Here, $\beta = v/c = 1/n(\lambda)$, and we obtain a minimum energy $E_{e,\min}$ of 158 keV. Very similar values are obtained for other types of crystals.

The spectrum of the Cherenkov radiation is well described by the Frank-Tamm formula [50],

$$\frac{dN_{\text{ph}}}{d\lambda\, dx} = \frac{2\pi\alpha}{\lambda^2}\left(1 - \frac{c^2}{v^2 n^2(\lambda)}\right), \tag{5}$$

where dN_{ph} is the number of Cherenkov photons emitted in the wavelength range $d\lambda$ while the electron travels the elementary path dx in the medium. v is the speed of the electron, and $\alpha = e^2/(\hbar c) \simeq 1/137$. To obtain the total number of photons emitted, it is necessary to integrate over the path of the electron. Expressing the path x in terms of the instant kinetic energy E_e, the integration reads

$$\frac{dN_{ph}}{d\lambda}(E_{e,0}) = \int_{E_{e,\min}}^{E_{e,0}} \frac{dN_{ph}}{d\lambda\, dx}(E_e)\left|\frac{dx}{dE_e}\right| dE_e, \tag{6}$$

where $E_{e,0}$ is the initial energy of an electron. This calculation is straightforward using tabulated values of electron ranges $\ell_e(E_{e,0})$ in CaF_2 [51] and the correspondence $x(E) = \ell_e(E_{e,0}) - \ell_e(E)$.

B. Origin of Cherenkov radiation and yield of various processes

Electrons of large enough energy may originate from the following processes: (i) β^- decay with sufficiently large energy Q_β released, (ii) highly energetic conversion electrons (CEs) accompanying radioactive transformation of nuclei, and (iii) highly energetic γ rays, which interact with the crystal via the photoelectric effect (predominantly below 100 keV), Compton scattering (100 keV–10 MeV) and pair production (above 10 MeV). We will now look at these processes more closely and estimate the yield of Cherenkov radiation.

(i) *β electrons* are characterized by a continuous energy spectrum, which may be described by the Fermi law [52]

$$\frac{dN_\beta}{dE_{e,0}}(E_{e,0}) = C\, F(z, E_{e,0})\sqrt{E_{e,0}^2 + 2E_{e,0}m_e c^2} \times (Q_\beta - E_{e,0})^2(E_{e,0} + m_e c^2), \tag{7}$$

where C is a normalization constant and z is the atomic number of the daughter nucleus. The Fermi function $F(z, E_{e,0})$ describes the Coulomb interaction between the emitted electron and the nucleus; see Ref. [52] for an explicit expression. The average Cherenkov yield of β electrons obtained in a decay with end-point energy Q_β is given by

$$\frac{dN_{ph,\beta}}{d\lambda}(Q_\beta) = \int_{E_{e,\min}}^{Q_\beta} \frac{dN_{ph}}{d\lambda}(E_{e,0})\frac{dN_\beta}{dE_{e,0}}(E_{e,0})dE_{e,0}, \tag{8}$$

where $\frac{dN_{ph}}{d\lambda}(E_{e,0})$ is given by Eq. (6).

(ii) *Conversion electrons* are characterized by their discrete energy spectrum. Therefore, their yield may be calculated directly by formula (6).

(iii) *High-energy γ rays* accompanying radioactive decay of nuclei may produce secondary high-energy electrons via Compton scattering, photoabsorbtion, and pair production. In the experiment considered here, all γ rays are below 3 MeV in energy. On the other hand, γ rays with energy below $E_{e,\min} = 158$ keV cannot produce electrons of sufficiently high energy to contribute to the Cherenkov radiation. The most efficient scattering process between a few 100 keV and a few MeV, and the only one considered here, is Compton scattering.

The energy $E_{e,0}$ of a scattered electron is connected with the energy E_γ of the incident γ ray and the scattering angle θ as

$$1 - \frac{E_{e,0}}{E_\gamma} = \frac{1}{1 + \frac{E_\gamma}{m_e c^2}(1 - \cos\theta)}. \tag{9}$$

To find the minimum γ ray energy E_γ required to generate an electron with energy $E_{e,\min} = 158$ keV (at the threshold to emit Cherenkov radiation), we set $\theta = 180^\circ$ and obtain $E_{\gamma,\min} = 295$ keV.

The differential cross section of Compton scattering into the elementary energy of the scattered electron may be given with the help of the Klein-Nishina differential cross section into the elementary solid angle and relation (9) between the scattering angle and the energy of the scattered electron. The cross section reads

$$\frac{d\sigma}{dE_{e,0}}(E_\gamma, E_{e,0}) = \pi r_e^2 \frac{m_e c^2}{E_\gamma^2}\left[\frac{E'_\gamma}{E_\gamma} + \frac{E\gamma}{E'_\gamma} + \left(\frac{m_e c^2}{E'_\gamma} - \frac{m_e c^2}{E_\gamma}\right)^2 - 2\left(\frac{m_e c^2}{E'_\gamma} - \frac{m_e c^2}{E_\gamma}\right)\right], \tag{10}$$

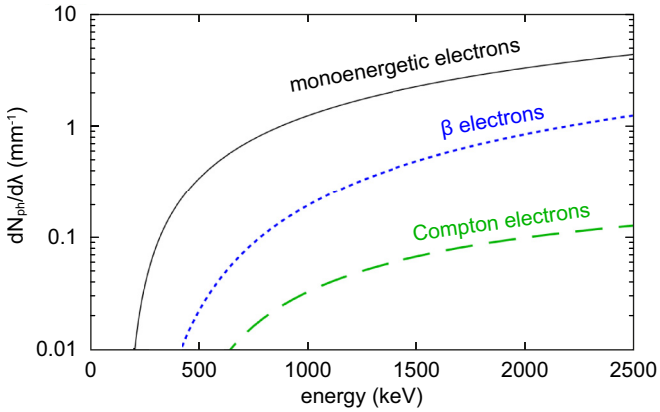

FIG. 5. Comparison of the average number of Cherenkov photons emitted within a 1-nm-wide spectral window near $\lambda = 160$ nm on average by one monoenergetic electron of energy $E_{e,0}$ (black, solid), of β electrons emitted in a decay with Q_β (blue, dotted), and Compton electrons emerging from scattering with γ rays of energy E_γ (green, dashed). The path length of γ rays in the crystal has been taken as $\ell_\gamma = 5$ mm.

where $r_e = e^2/(m_e c^2)$ is the classical electron radius, and $E'_\gamma = E_\gamma - E_{e,0}$ is the energy of the scattered γ ray.

The range of high-energy γ rays in the crystal medium is much larger than the actual size of our crystals. For example, the probability of a 300-keV γ ray to interact with the CaF_2 crystal over a path of 5 mm length is only about 15%; this value is even smaller for γ rays of higher energy [47]. This fact allows us to neglect the attenuation of γ rays, as well as the interaction of scattered γ rays with the medium. Assuming a path length of $\ell_\gamma = 5$ mm in the crystal, we estimate the average yield of a single γ ray with energy E_γ born in the crystal as

$$\frac{dN_{ph,\mathrm{Compt}}}{d\lambda}(E_\gamma) = n_e \ell_\gamma \int_{E_{e,\min}}^{E_{e,\max}(E_\gamma)} \frac{d\sigma}{dE_{e,0}}(E_\gamma, E_{e,0}) \times \frac{dN_{ph}}{d\lambda}(E_{e,0})\, dE_{e,0}, \quad (11)$$

where $E_{e,\max}(E_\gamma)$ is given by Eq. (9) at $\theta = 180^\circ$.

The Cherenkov yields of the three different processes discussed above are compared in Fig. 5.

C. Ingrowth of daughters and contamination with ^{232}U

The Cherenkov radiation shown in Fig. 3 cannot be caused directly by the α decay of pure ^{233}U, as this decay is not accompanied by a significant number of conversion electrons or γ rays of sufficiently high energy. Instead, the Cherenkov radiation originates from activity in the sequence of short-lived ^{229}Th daughters, namely (i) the β decay of ^{225}Ra, ^{213}Bi, and ^{209}Pb, (ii) conversion electrons, and (iii) the high-energy γ rays of various daughters, e.g., ^{213}Bi.

The ^{233}U source used for the measurements was not purified, and daughters have been building up for the past 45 years (measured by inductively coupled plasma mass spectrometry, ICP-MS). Chemical purification of the ^{233}U is expected to be capable of removing 99.5% of the thorium. Such a preparation would reduce the Cherenkov radiation initially by a factor of 200, with a very slow buildup over the ^{229}Th lifetime.

The ^{233}U material was obtained by neutron irradiation of ^{232}Th through the steps $^{232}\mathrm{Th} + n \rightarrow {}^{233}\mathrm{Th} \xrightarrow{\beta} {}^{233}\mathrm{Pa} \xrightarrow{\beta} {}^{233}\mathrm{U}$. Depending on the details of the breeding process, the ^{233}U contains non-negligible amounts of ^{232}U as a by-product of the neutron irradiation. The short half life of ^{232}U (70.6 yr) and its first daughter ^{228}Th (1.9 yr) lead to a high activity of the entire chain, which includes strong γ ray emission. Unlike the ^{233}U chain, which "pauses" at ^{229}Th for nearly 8000 years, the ^{232}U chain proceeds down to the stable ^{208}Pb on time scales comparable to the duration of the experiment.

Using γ spectroscopy, the content of ^{232}U in the ^{233}U plate source used here has been determined to 11.6(1.0) ppm. At this level, the γ radiation of the ^{232}U chain clearly dominates over the ^{233}U chain; the same is true for β decays. It is thus important that the spectroscopy experiment proposed in the main text be carried out with ^{233}U material almost free of ^{232}U.

V. SIGNAL-TO-NOISE RATIO OF A FUTURE EXPERIMENT

We will now attempt to model a future spectroscopy experiment. We assume a ^{233}U:CaF_2 crystal of density $\rho_{CaF_2} = 3.18$ g/cm^3, thickness $d = 5$ mm, and ^{233}U doping concentration $n_U = 5 \times 10^{-4}$; such concentrations can easily be achieved. Note that n_U denotes the amount of uranium ions per crystal unit cell, where, for simplicity, we assume a unit cell to contain one Ca ion and two F ions, $M_{CaF_2} = 78.075$ g/mol. The crystallographic unit cell would contain four Ca ions and eight F ions. Further, we assume the contamination of ^{232}U to be $C_{232} = 10$ ppm, and we assume that $t = 100$ days have elapsed since the last removal of thorium (both ^{228}Th and ^{229}Th) from the source. The ^{228}Th and ^{229}Th chains are in secular equilibrium. Such a crystal of $10 \times 5 \times 2$ mm^3 would have a ^{233}U activity of 170 kBq (identical to the source used in Ref. [18]) plus 4 kBq from the ^{232}U chain. The crystal absorption parameter is taken as $\xi_U(160\ \mathrm{nm}) = 6.3 \times 10^{-5}$ cm.

Concerning the experimental setup, we consider a standard VUV spectrometer, where the crystal is imaged onto the entrance slit of the spectrometer using 1:1 imaging optics with a solid angle coverage of 0.14% (e.g., $2f = 200$ mm, mirror diameter $d = 30$ mm) and a mirror reflectivity in the UV of 80%. The entrance slit has a height h of 8 mm and a width w of 330 μm, and is imaged onto the detector with a spherically concave grating. The grating is assumed to have a diffraction efficiency of 20%, and the quantum efficiency of the detector is 30%. The total detection efficiency as the product of solid angle, mirror reflectivity, and grating and detector efficiencies is $D = 6.7 \times 10^{-5}$. A charge-coupled device (CCD) camera allows continuous measurement of the entire spectral region of interest. A grating with 1200 grooves/mm translates the 330-μm slit width to 1.0 nm spectral width. The spectrum, captured by a standard CCD detector (8 mm height, 30 mm width), would cover 90 nm, conveniently matching the window

between the CaF_2 transparency cutoff at 125 nm and the onset of α-radiation induced radioluminescence at 220 nm.

A. Signal amplitude

The expression for the flux Φ_γ given in Eq. (2) relies on a number of simplifications. We will show now that these simplifications are justified for reasonable parameters. At first, the factor ξ_U stems from an integration over all sources of isomer γ rays,

$$\int_0^d n_U\, e^{-n_U x/\xi_U(\lambda)}\, dx, \tag{12}$$

where we assume n_U to be constant across the sample. For $d = \infty$, the integration yields exactly $\xi_U(\lambda)$. For the parameters chosen above, the integral is $0.981\xi_U(\lambda)$, and more generally, the approximation is justified for $n_U d/\xi_U(\lambda) \gg 1$.

Second, the integral is only one dimensional, assuming all VUV γ rays propagate perpendicular to the crystal surface. In correct terms, the expression of Eq. (2) would read

$$\frac{d\Phi_\gamma}{d\Omega}(\vartheta = 0^\circ) = \frac{1}{4\pi}\xi_U(\lambda) \times \frac{\rho_{\text{crystal}}}{M_{\text{crystal}}} \times N_A \frac{\ln(2)}{t_{1/2}} \times R \times B, \tag{13}$$

which would give a maximum flux of $d\Phi_\gamma/d\Omega(\vartheta = 0) = 340/(\text{s} \times \text{cm}^2 \times \text{srad})$. This geometric simplification is certainly justified, as we consider light collection optics placed far away from the crystal, capturing only photons within a small solid angle. For the parameters given above, the largest deviation from normal incidence is $\vartheta = 4.3^\circ$.

As a third simplification, we assume that light absorption is dominated by the uranium content and not by the absorption of the CaF_2 crystal itself. In this way, the expression in Eq. (2) becomes independent of the doping concentration n_U and crystal thickness d.

By far the largest uncertainty in Φ_γ stems from the uncertainty in the probability B to populate the isomer and the unknown magnitude of competing nonradiative decay channels. The possibility of nonradiative decay is captured in the quantity R, which denotes the probability of radiative decay. Using values of $B = 2\%$, $R = 1$, and $\Phi_\gamma = 4200/(\text{s} \times \text{cm}^2)$, the rate of isomer γ rays at the detector is

$$\Phi'_\gamma = \Phi_\gamma \times h \times w \times D, \tag{14}$$

and we obtain $\Phi'_\gamma = 0.0075\ \text{s}^{-1}$ for the experimental specifications stated above.

In the following, we will compare this signal amplitude to various sources of background noise.

B. Cherenkov radiation from ^{233}U γ rays

The α decay of ^{233}U is accompanied by only very few conversion electrons and γ rays of sufficiently high energy to generate Cherenkov light; see Tables I and II. Using the models derived in Sec. IV, we calculate that in total, there are on average only $N_{233} = 2.6 \times 10^{-6}$ Cherenkov photons emitted into a 1-nm interval at $\lambda = 160$ nm per disintegration of ^{233}U. Comparing the emission of Cherenkov photons and isomer γ rays,

$$\frac{R_{\text{Ch},233}}{R_\gamma} = \frac{N_{233}}{R \times B}, \tag{15}$$

we find that for values $R > 10^{-4}$, the number of emitted isomer γ rays exceeds the number of Cherenkov photons.

TABLE I. Coarse-grained spectrum of conversion electrons with energies above $E_{e,\text{min}} = 158$ keV that appear in the decay of ^{233}U. The value of $dN_{\text{ph}}/d\lambda$ is given for a spectral window of 1 nm width. Values are taken from Ref. [42].

$E_{e,0}$ (keV)	$\overline{E_{e,0}}$ (keV)	Occurrence per 10^6 disintegrations	$\frac{dN_{\text{ph}}}{d\lambda}$ at 160 nm per 10^6 disintegrations
158–200	178	39.78	0.081
200–300	235	68.25	1.8
300–400	314	6.79	0.63
> 400	469	0.0194	0.006

C. Cherenkov radiation from β decay in the ^{229}Th chain

There are four β decays in the decay chain of ^{233}U, one of which constitutes only a weak decay channel. From the ENSDF database [53], we extract the decay probability and released energy Q_β; see Table III. All of the values of Q_β are above $E_{e,\text{min}} = 158$ keV.

Next, we use the ESTAR values provided by NIST [51] to calculate the path lengths of the electrons in CaF_2. Employing the continuous slowing-down approximation (CSDA), we obtain exemplary path lengths s of $s(300\ \text{keV}) = 0.33$ mm, $s(1\ \text{MeV}) = 1.7$ mm, and $s(2\ \text{MeV}) = 3.8$ mm. As a conservative simplification, we will assume that all electron paths are contained within the crystal.

We then employ Eq. (8) to calculate the average number of Cherenkov photons within a 1-nm spectral window around 160 nm, created along the entire chain of ^{229}Th daughters. We find that 100 decays of ^{229}Th are accompanied by the creation of 40 Cherenkov photons per nm in the wavelength region of interest.

D. Cherenkov radiation from γ radiation and conversion electrons in the ^{229}Th chain

As a next step, we go through the entire decay chain of ^{229}Th down to ^{205}Tl and, for each of the 10 decay steps, extract the

TABLE II. Coarse-grained spectrum of γ rays with energies above $E_{\gamma,\text{min}} = 295$ keV that appear in the decay of ^{233}U. Values are taken from Ref. [42].

E_γ (keV)	$\overline{E_\gamma}$ (keV)	Occurrence per 10^6 disintegrations	$\frac{dN_{\text{ph}}}{d\lambda}$ at 160 nm per 10^6 disintegrations
295–350	319	118.6	0.0019
350–500	373	10.4	0.0037
500–750	560	0.6	0.033

TABLE III. List of β decays occurring in the decay chain of ^{229}Th.

Decay	Q_β (keV)	Occurrence (%)	$\frac{dN_{ph}}{d\lambda}$ at 160 nm per 100 decays of ^{229}Th
^{209}Tl → ^{209}Pb	1827	2.04	1.4
^{213}Bi → ^{213}Po	1423	64.8	27.5
^{213}Bi → ^{213}Po	983	30.2	5.5
^{209}Pb → ^{209}Bi	644	100	5.4
^{225}Ra → ^{225}Ac	356	31.2	0.13
^{225}Ra → ^{225}Ac	316	68.8	0.14

γ ray emission lines with energies above $E_{\gamma,\min} = 295$ keV. Table IV lists all such γ ray lines that have a probability of more than 0.1% to appear in succession to a disintegration of ^{229}Th. Only one transition, located at 440.4 keV, has a probability of more than a few percent. While we listed only transitions with probabilities above 0.1% here, we checked that a summation over all the weaker transitions, as they appear, e.g., in the decay of ^{225}Ac, can safely be neglected.

An equivalent search is performed for conversion electrons (not listed here). We estimate the total contribution of conversion and Compton electrons to the Cherenkov radiation background to be at the level of 0.74 and 0.15 photons per nm per 100 ^{229}Th decays.

The Cherenkov photons are identical to the isomer γ rays in wavelength, location of origin, and propagation to the detector. The ratio between the emission rates of Cherenkov photons vs isomer γ rays for a decay of ^{233}U reads

$$\frac{R_{\mathrm{Ch},229}}{R_\gamma} = \frac{t \times \lambda_{229} \times N_{229}}{R \times B}. \tag{16}$$

Here, $\lambda = \ln(2)/t_{1/2}$ is the decay constant. For $B = 2\,\%$, $R = 1$, $N_{229} = 0.41$ Cherenkov photons in the wavelength region of interest, and a time of $t = 100$ days allowed for the ingrowth of ^{229}Th, we obtain a value of 4.9×10^{-4}.

E. Cherenkov radiation from ^{232}U contamination

The production of ^{233}U is plagued by the parasitic appearance of ^{232}U. Even for contaminations at the ppm level, the activity of the material can be dominated by the ^{232}U chain.

TABLE IV. List of γ ray lines with energies above $E_{\gamma,\min} = 295$ keV and a probability above 0.1% to appear in the decay chain of ^{229}Th.

Decay	E_γ (keV)	Occurrence (%)
^{209}Tl → ^{209}Pb	1566.9	2.08
^{213}Bi → ^{213}Po	1100.2	0.27
^{213}Bi → ^{213}Po	807.4	0.29
^{209}Tl → ^{209}Pb	465.1	2.02
^{225}Ac → ^{221}Fr	452.2	0.11
^{213}Bi → ^{213}Po	440.4	25.5
^{221}Fr → ^{217}At	410.6	0.12
^{213}Bi → ^{213}Po	323.7	0.16

TABLE V. List of β decays occurring in the decay chain of ^{228}Th with energies above 158 keV and probabilities above 1%.

Decay	Q_β (keV)	Occurrence (%)	$\frac{dN_{ph}}{d\lambda}$ at 160 nm per 100 decays of ^{229}Th
^{212}Bi → ^{212}Po	2252.1	55.3	57
^{208}Tl → ^{208}Pb	1801.3	17.7	12
^{212}Bi → ^{212}Po	1524.8	4.50	2.19
^{208}Tl → ^{208}Pb	1523.9	7.96	3.92
^{208}Tl → ^{208}Pb	1290.5	8.71	3
^{208}Tl → ^{208}Pb	1038.0	1.14	0.23
^{212}Bi → ^{212}Po	739.4	1.44	0.12
^{212}Bi → ^{212}Po	631.4	1.90	0.09
^{212}Pb → ^{212}Bi	569.9	13.3	0.42
^{212}Pb → ^{212}Bi	331.3	81.7	0.22

The parent ^{232}U undergoes α decay into ^{228}Th (half life 1.9 yr) without significant emission of high-energy γ rays.

A list of β decays in the ^{228}Th chain is given in Table V. We find that the decay of 100 ^{228}Th nuclei is accompanied by 79 Cherenkov photons emitted by β electrons in a 1-nm interval near 160 nm.

We then take a look at the γ rays emitted along the ^{228}Th chain; see Table VI. In analogy to the ^{229}Th decay chain, we estimate the total contribution of conversion and Compton electrons to the Cherenkov background to be at the level of 0.75 and 5.4 photons per nm per 100 ^{228}Th decays. In total, we have 85 Cherenkov photons emitted in a 1-nm interval near 160 nm for every 100 decays of ^{228}Th, produced by all its daughters.

Assuming t to be much shorter than the half life of ^{228}Th, the ratio of Cherenkov photons emitted per isomer γ ray reads

$$\frac{R_{\mathrm{Ch},228}}{R_\gamma} = \frac{t \times \lambda_{228} \times \frac{\lambda_{232}}{\lambda_{233}} \times N_{228} \times C_{232}}{R \times B} \tag{17}$$

and takes a value of 0.096 for $B = 2\%$, $R = 1$, an ingrowth time of $t = 100$ days, and a contamination of $C_{232} = 10$ ppm.

F. Cherenkov spectrum

So far, we have presented only the Cherenkov emission $dN_{ph}/d\lambda$ near the expected wavelength of 160 nm. To com-

TABLE VI. List of γ ray lines with energies above $E_{\gamma,\min} = 295$ keV and a probability above 1% to appear in the decay chain of ^{228}Th.

Decay	E_γ (keV)	Occurrence (%)
^{212}Bi → ^{212}Po	1620.7	1.51
^{208}Tl → ^{208}Pb	860.5	4.46
^{212}Bi → ^{212}Po	785.4	1.11
^{212}Bi → ^{212}Po	727.3	6.65
^{208}Tl → ^{208}Pb	583.2	30.6
^{208}Tl → ^{208}Pb	510.7	8.10
^{212}Pb → ^{212}Bi	300.1	3.18

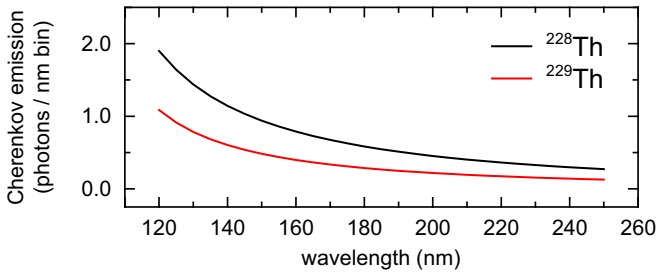

FIG. 6. Spectral shape of the Cherenkov emission in CaF_2, calculated as photons per one decay along the entire chain of the respective thorium isotope, within a 1-nm spectral window.

plete the picture, we calculate the entire Cherenkov emission spectrum between 120 and 250 nm; see Fig. 6. The emission amplitude increases only mildly towards the UV cutoff around 120 nm.

G. Detector noise

State-of-the-art CCD detectors can be cooled to $-100\,^{\circ}$C, which reduces the dark noise to a level that is entirely negligible in comparison to the read-out noise of typically less than one electron. Events related to the impact of highly energetic particles (e.g., of cosmic origin or from environmental radioactivity) are the dominant disturbance. A routine to remove such events from the data set is required.

We define a parameter $\Omega = t_{\mathrm{exp}} \times A$, where t_{exp} is the exposure time of a single image and A is the binning area of the CCD chip. The binning area A can be matched to the average area of "cosmic" events. We find that for $\Omega = 3.3\ \mathrm{s} \times \mathrm{cm}^2$, about 5% of all data points are contaminated by cosmic events; this value has proven to be a good choice for the detection of small signals. Using this value of Ω, a subarea of the CCD chip corresponding to a spectral width of 1.0 nm could thus be integrated over 125 s. The isomer γ ray signal integrated during this time (assuming $B = 2\%$ and $R = 1$) is already comparable to the read-out noise.

H. Measurement time and nonradiative decay probability

Summing over all contributions, the ratio between Cherenkov photons emitted in the 1-nm window at 160 nm and the isomer γ rays reads

$$\frac{R_{\mathrm{Ch}}}{R_\gamma} = \frac{N_{233} + t \times (\lambda_{229}\, N_{229} + \lambda_{228}\, \frac{\lambda_{232}}{\lambda_{233}}\, N_{228}\, C_{232})}{R \times B}. \quad (18)$$

Only for entirely unrealistic times t smaller than a few minutes does the decay of ^{233}U dominate over the two thorium chains, and only for very low concentrations $C_{232} < 0.5$ ppm does the ^{229}Th chain dominate over the ^{228}Th chain. We have thus identified the β decays in the chain of ^{232}U contamination as the main source of Cherenkov radiation; refer to Table VII for a summary.

We will now calculate the integration time T it takes for the integrated isomer signal to become comparable to the noise of the Cherenkov background,

$$\Phi'_\gamma \times T \simeq \sqrt{\Phi'_\gamma \times \frac{R_{\mathrm{Ch}}}{R_\gamma} \times T}, \quad (19)$$

or

$$T \simeq \frac{1}{\Phi'_\gamma} \times \frac{R_{\mathrm{Ch}}}{R_\gamma}. \quad (20)$$

Taking the detected signal amplitude of Φ'_γ from Eqs. (2) and (14), R_{Ch}/R_γ from Eq. (18), and assuming $t = 100$ days, $C_{232} = 10$ ppm, $B = 2\%$, and a radiative decay probability of only $R = 1\%$, we obtain a characteristic integration time scale of $T = 1.5$ days.

The comparatively short measurement time is very promising: the isomer emission can be detected within a few days of measurement time even if only 1% of the isomers undergo radiative de-excitation, or, equivalently, if B was two orders of magnitude smaller than expected.

To give a second example, even for $R = 10^{-3}$, a reduced contamination of $C_{232} = 3$ ppm, and a shorter ingrowth time of $t = 30$ days, the isomer emission could be measured within a few weeks.

Note that, apart from the light throughput of the spectrometer, t and C_{232} are the only tunable parameters that have an effect on T. Note also that T is independent of the spectrometer slit width, as the values of N scale approximately linear with the spectral window defined by the slit width. Importantly, T scales as $(R \times B)^{-2}$. Note also that the ratio R_{Ch}/R_γ calculated above is exactly the same for the two approaches of surface implantation, using a thin layer of ^{233}U, and direct doping of the uranium into the crystal.

TABLE VII. Summary of the amount of Cherenkov photons created in a 1-nm spectral window centered at 160 nm, originating from β decay, conversion electrons (CEs), and Compton scattering. N is the sum of these three processes.

Origin	β decay	CE	Compton	N
^{233}U decay		2.5×10^{-6}	3.9×10^{-8}	2.5×10^{-6}
^{229}Th chain	0.40	7.4×10^{-3}	1.5×10^{-3}	0.41
^{228}Th chain	0.79	7.5×10^{-3}	0.054	0.85

VI. ORIGIN OF THE RADIOLUMINESCENCE FEATURE AROUND 280 NM

The major fraction of ^{233}U-induced radioluminescence in CaF_2 is radiated between 220 and 360 nm, as shown in Fig. 3. We will now attempt to identify the kind of radiation that causes this scintillation. There are a number of candidates: Th recoil ions implanted into the crystal, α and β particles, γ rays, as well as electrons and x rays from secondary processes. To quantify the individual contributions, we place a commercial CaF_2 crystal (5 mm thickness, 25 mm diameter) in close proximity to a ^{233}U sample. We insert three different absorbers in between the radiation source and the crystal and record the emission spectrum.

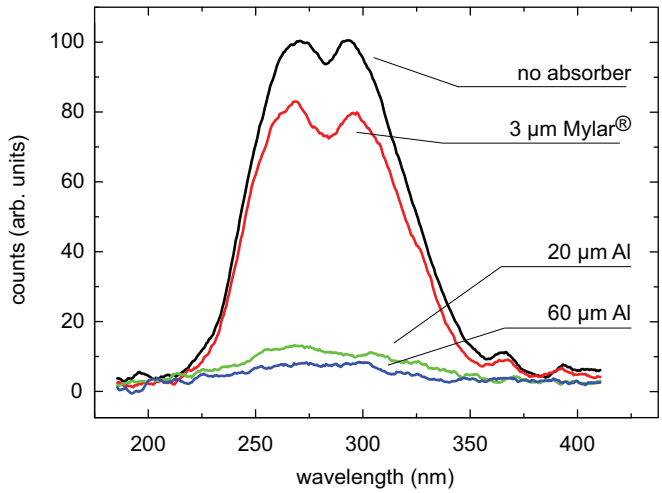

FIG. 7. Radioluminescence spectrum of CaF_2, brought into close proximity of a ^{233}U source. Shielding the radiation by a thin Mylar® foil (stops only Th nuclei) reduces the signal by 20%, and shielding with aluminum foils (stop also α particles, yet transmits β electrons and γ rays) reduces the signal to below 10%.

A 3-μm Mylar® foil securely absorbs the Th recoil ions, but transmits nearly all of the 4.8-MeV α particles (27-μm range) and all of the β electrons, γ rays, and x rays. With this foil in place, we observe a 20% drop in signal amplitude; see Fig. 7.

We then substitute the Mylar® foil by 20 μm of aluminum, which corresponds to the range of α particles. The foil transmits 99.4% of all γ rays at an energy of 30 keV [47] and all of the β particles in question. The signal drops to 10%, and it drops further to 5.5% as the Al layer thickness is increased to 60 μm.

The measurement suggests that the signal is caused predominantly by α particles, with much smaller contributions from recoil nuclei and γ rays. This finding is consistent with the fact that more than 95% of the energy deposited into the crystal from radioactive decay of our ^{233}U source is via α particles. Note that the presence of the ^{232}U chain increases the overall activity, but the partition of the energy released into α particles, β particles, and γ rays is roughly equal to the ^{233}U chain.

To further study the effect of high-energy γ radiation, we employ a more powerful source: A commercial CaF_2 sample is placed directly into the core of a shut-down TRIGA Mark II reactor, where it is subjected to a massive flux of γ rays. α and β particles are shielded by the water surrounding the fuel rods. After 15 h of exposure, the crystal is quickly transferred into the spectrometer, but no signal resembling the spectrum of Fig. 7 is observed. We conclude that, in absence of crystal contaminations, γ radiation does not induce noticeable long-lived defects.

To complete our studies, we subject the CaF_2 sample to the radiation of a pure α emitter. We use a ^{241}Am source with an activity of 5.5 MBq (kindly provided by M. Fugger, Atominstitut, Vienna), the sample is exposed to this radiation for 45 h. The penetration depth of the 5.5-MeV α particles is estimated to be 15 μm. After an integrated bombardement of 2×10^{11} α particles per cm^2, no damage or coloring of the crystal is observed, nor is the optical transmission reduced. A measurement of the luminescence spectrum begins 10 min after the end of exposure, but no signal of long-lived defects is observed between 120 and 500 nm. A similar experiment with MgF_2 returns the same null result.

VII. CONCLUSION

To conclude, we proposed a new method to detect and measure the VUV γ ray of the ^{229}Th isomer from the α decay of ^{233}U in VUV-transparent crystals. The expected flux of isomer γ rays is two orders of magnitude larger compared to experiments using thin films of ^{233}U. We found that radioluminescence induced by the α decay is spectrally separated from the expected isomer wavelength region. This region, however, is covered by Cherenkov radiation, induced predominantly by the β decay of ^{228}Th and ^{229}Th daughters. The flux of isomer γ rays extracted from the crystal is so large that, even if the probability of radiative de-excitation of the isomer is only 1%, the signal can be discriminated from the broad Cherenkov radiation after a spectroscopy measurement time of only a few days. Assuming a reduced ^{232}U contamination of only a few ppm and a measurement time of a few weeks, the isomer emission can be observed even if the radiative de-excitation channel amounts to only 0.1%.

ACKNOWLEDGMENTS

We thank J. Schwestka, V. Schauer, and V. Rosecker for preparation of uranium samples. We greatly appreciate fruitful discussions with E. Peik, L. von der Wense, and P. G. Thirolf. This work has received funding from the ERC project 258604-NAC, the FWF project I1602, and from the European Union's Horizon 2020 Research and Innovation Programme under Grant Agreement No. 664732 "nuClock".

[1] L. A. Kroger and C. W. Reich, Nucl. Phys. A **259**, 29 (1976).
[2] C. W. Reich and R. G. Helmer, Phys. Rev. Lett. **64**, 271 (1990).
[3] D. G. Burke, P. E. Garrett, T. Qu, and R. A. Naumann, Phys. Rev. C **42**, R499 (1990).
[4] R. G. Helmer and C. W. Reich, Phys. Rev. C **49**, 1845 (1994).
[5] B. R. Beck, J. A. Becker, P. Beiersdorfer, G. V. Brown, K. J. Moody, J. B. Wilhelmy, F. S. Porter, C. A. Kilbourne, and R. L. Kelley, Phys. Rev. Lett. **98**, 142501 (2007).
[6] L. v. d. Wense, B. Seiferle, M. Laatiaoui, J. B. Neumayr, H.-J. Maier, H.-F. Wirth, C. Mokry, J. Runke, K. Eberhardt, C. E. Düllmann *et al.*, Nature (London) **533**, 47 (2016).

[7] A. M. Dykhne and E. V. Tkalya, JETP Lett. **67**, 549 (1998).
[8] E. Peik and C. Tamm, Europhys. Lett. **61**, 181 (2003).
[9] V. V. Flambaum, Phys. Rev. Lett. **97**, 092502 (2006).
[10] W. G. Rellergert, D. DeMille, R. R. Greco, M. P. Hehlen, J. R. Torgerson, and E. R. Hudson, Phys. Rev. Lett. **104**, 200802 (2010).
[11] E. V. Tkalya, Phys. Rev. Lett. **106**, 162501 (2011).
[12] C. J. Campbell, A. G. Radnaev, A. Kuzmich, V. A. Dzuba, V. V. Flambaum, and A. Derevianko, Phys. Rev. Lett. **108**, 120802 (2012).
[13] S. Das, A. Pálffy, and C. H. Keitel, Phys. Rev. C **88**, 024601 (2013).
[14] G. A. Kazakov, A. N. Litvinov, V. I. Romanenko, L. P. Yatsenko, A. V. Romanenko, M. Schreitl, G. Winkler, and T. Schumm, New J. Phys. **14**, 083019 (2012).
[15] B. R. Beck *et al.*, Report No. LLNL-PROC-415170, 2009.
[16] A. M. Dykhne and E. V. Tkalya, JETP Lett. **67**, 251 (1998).
[17] E. Ruchowska *et al.*, Phys. Rev. C **73**, 044326 (2006).
[18] X. Zhao, Y. N. Martinez de Escobar, R. Rundberg, E. M. Bond, A. Moody, and D. J. Vieira, Phys. Rev. Lett. **109**, 160801 (2012).
[19] E. Peik and K. Zimmermann, Phys. Rev. Lett. **111**, 018901 (2013).
[20] E. V. Tkalya, C. Schneider, J. Jeet, and E. R. Hudson, Phys. Rev. C **92**, 054324 (2015).
[21] J. Jeet, C. Schneider, S. T. Sullivan, W. G. Rellergert, S. Mirzadeh, A. Cassanho, H. P. Jenssen, E. V. Tkalya, and E. R. Hudson, Phys. Rev. Lett. **114**, 253001 (2015).
[22] A. Yamaguchi, M. Kolbe, H. Kaser, T. Reichel, A. Gottwald, and E. Peik, New J. Phys. **17**, 053053 (2015).
[23] C. J. Campbell, A. G. Radnaev, and A. Kuzmich, Phys. Rev. Lett. **106**, 223001 (2011).
[24] O. A. Herrera-Sancho, N. Nemitz, M. V. Okhapkin, and E. Peik, Phys. Rev. A **88**, 012512 (2013).
[25] H. Kikunaga, T. Suzuki, M. Nomura, T. Mitsugashira, and A. Shinohara, Phys. Rev. C **84**, 014316 (2011).
[26] S. L. Sakharov, Phys. At. Nucl. **73**, 1 (2010).
[27] S. Stellmer, M. Schreitl, and T. Schumm, Sci. Rep. **5**, 15580 (2015).
[28] E. V. Tkalya, A. N. Zherikhin, and V. I. Zhudov, Phys. Rev. C **61**, 064308 (2000).
[29] F. F. Karpeshin and M. B. Trzhaskovskaya, Phys. Rev. C **76**, 054313 (2007).
[30] P. V. Borisyuk, O. S. Vasilyev, A. V. Krasavin, Y. Yu. Lebedinskii, V. I. Troyan, and E. V. Tkalya, Physica Status Solidi (c) **12**, 1333 (2015).
[31] E. Browne and J. K. Tuli, Nucl. Data Sheets **109**, 2657 (2008).
[32] D. S. Richardson, D. M. Benton, D. E. Evans, J. A. R. Griffith, and G. Tungate, Phys. Rev. Lett. **80**, 3206 (1998).
[33] G. M. Irwin and K. H. Kim, Phys. Rev. Lett. **79**, 990 (1997).
[34] E. Browne, E. B. Norman, R. D. Canaan, D. C. Glasgow, J. M. Keller, and J. P. Young, Phys. Rev. C **64**, 014311 (2001).
[35] I. Moore, I. Ahmad, K. Bailey, D. L. Bowers, Z.-T. Lu, T. P. O'Connor, and Z. Yin, Argonne Physics Division Report No. PHY-10990-ME-2004, 2004 (unpublished).
[36] T. T. Inamura and H. Haba, Phys. Rev. C **79**, 034313 (2009).
[37] H. Kikunaga, Y. Kasamatsu, H. Haba, T. Mitsugashira, M. Hara, K. Takamiya, T. Ohtsuki, A. Yokoyama, T. Nakanishi, and A. Shinohara, Phys. Rev. C **80**, 034315 (2009).
[38] J. T. Burke, E. L. Swanberg, R. J. Casperson, and D. Thomas, Report. No. LLNL-TR-463538, 2010 (unpublished).
[39] L. v. d. Wense, P. G. Thirolf, D. Kalb, and M. Laatiaoui, J. Instrum. **8**, P03005 (2013).
[40] L. v. d. Wense, B. Seiferle, M. Laatiaoui, and P. G. Thirolf, Eur. Phys. J. A **51**, 29 (2015).
[41] M. P. Hehlen, R. R. Greco, W. G. Rellergert, S. T. Sullivan, D. DeMille, R. A. Jackson, E. R. Hudson, and J. R. Torgerson, J. Lumin. **133**, 91 (2013).
[42] NuDat 2.6 database, http://www.nndc.bnl.gov/nudat2/.
[43] W. A. Hargreaves, Phys. Rev. B **44**, 5293 (1991).
[44] L. Su, W. Yang, J. Xu, Y. Dong, and G. Zhou, J. Cryst. Growth **273**, 234 (2004).
[45] P. Rodnyi, *Physical Processes in Inorganic Scintillators* (CRC, Boca Raton, 1997).
[46] G. Kazakov, V. Schauer, J. Schwestka, S. Stellmer, J. Sterba, A. Fleischmann, L. Gastaldo, A. Pabinger, C. Enss, and T. Schumm, Nucl. Instrum. Methods Phys. Res. A **735**, 229 (2014).
[47] NIST database, http://www.nist.gov/pml/data/xraycoef/index.cfm.
[48] B. Srinivasan, Z. Hasan, N. B. Manson, and W. A. Runciman, J. Phys. C: Solid State Phys. **18**, 2381 (1985).
[49] A. Strasser and A. Vogler, Inorg. Chim. Acta **357**, 2345 (2004).
[50] J. V. Jelly, Prog. Nucl. Phys. **3**, 84 (1953).
[51] ESTAR program provided by NIST, http://physics.nist.gov/PhysRefData/Star/Text/ESTAR.html.
[52] P. Venkataramaiah, K. Gopala, A. Basavaraju, S. S. Suryanarayana, and H. Sanjeeviah, J. Phys. G: Nuclear Phys. **11**, 359 (1985).
[53] Evaluated Nuclear Structure Data File (ENSDF), provided by the National Nuclear Data Center at Brookhaven National Laboratory. Retrieved from the Laboratoire National Henri Bequerel at http://www.nucleide.org.